Organic Electronics 13 (2012) 373–376

Contents lists available at SciVerse ScienceDirect

Organic Electronics

journal homepage: www.elsevier.com/locate/orgel

Letter

In situ monitoring of photovoltaic properties in organic solar cells during thermal annealing

Chuan-Feng Shih *, Kuang-Teng Hung, Hsuan-Ta Wu, Sheng-Wen Fu, Hui-Ju Chen, Chu-Yun Hsiao

Department of Electrical Engineering and Center for Micro/Nano Science and Technology, National Cheng Kung University, Tainan 70101, Taiwan

ARTICLE INFO

Article history:
Received 16 September 2011
Received in revised form 20 October 2011
Accepted 21 November 2011
Available online 9 December 2011

Keywords:
In situ monitoring
Organic solar cells
Annealing

ABSTRACT

This paper reports a simple and useful technique that monitors the changes of poly(3-hexylthiophene) (P3HT):1-(3-methoxycarbonyl)-propyl-1-phenyl-(6,6)C_{61}-based organic solar cells (OSCs) during thermal annealing *in situ*. Thermal annealing was divided into five stages in which the variations of the cell parameters were obtained in detail. Annealing temperature that was higher than the glass transition temperature of P3HT (127 °C) was found critical to the improvement of open-circuit voltage. The initial rise of the short-circuit current was explained by *in situ* monitoring of the transport behaviors of electrons and holes. Finally, *in situ* monitoring was adopted to compare OSCs that were or were not solvent-annealed, indicating the effectiveness in optimizing, modeling and understanding in depth the effects of the thermal annealing of OSC with a blended active layer.

1. Introduction

Poly(3-hexylthiophene) (P3HT):1-(3-methoxycarbonyl)-propyl-1-phenyl-(6,6)C_{61} (PCBM)-based bulk heterojunction organic solar cells (OSCs) have achieved high power conversion efficiency (PCE) of ~5% [1]. Thermal annealing, control of the casting rate of the blended active layer, solvent annealing and the usage of a mixed solvent are key techniques to obtain a high efficiency [2–5]. Among these successful methods, thermal annealing is the most efficient way that has been used to further increase the PCE of a solvent-annealed OSC device [6]. Many efforts have been made to investigate the effect of temperature and time-scale on the thermal annealing. However, the results usually vary among laboratories for three reasons. First, the fabrication parameters of OSCs are considerably varied unintentionally during fabrication process. For example, the active layer is somewhat solvent-annealed during spin casting, which is usually performed in a closed space that is filled with organic vapor. In addition, damages associated with the deposition of metal and the patterning of ITO also alter the conclusions drawn about thermal annealing. Second, the phenomena that are involved in thermal annealing of the OSCs are complicated. Phase separation, clustering of PCBM, segregation, ordering of P3HT molecules and morphological changes all occur simultaneously during thermal annealing. Third, some fabrication processes differ among laboratories, such as the ramping rates of heating and cooling, the speed and step of spin-casting, and the P3HT:PCBM mixing ratio. Therefore, the influence of thermal annealing on OSCs is difficult to determine when all of these factors are considered. Many speculative claims have been made. Optimization of the PCE of OSCs by thermal annealing requires numerous experiments.

Recently, real-time scanning probe equipped with near-field spectroscopy, photoluminescence, Raman spectroscopy, glazing-angle X-ray diffraction, and synchrotron X-ray reflectivity spectroscopy have been used to explore the crystalline, optical and morphological changes of OSCs during thermal or solvent annealing [7–11]. Related results provide useful dynamic information that cannot be ob-

* Corresponding author. Tel.: +886 6 2757575x62398; fax: +886 6 2080687.
E-mail address: cfshih@mail.ncku.edu.tw (C.-F. Shih).

1566-1199/$ - see front matter © 2011 Elsevier B.V. All rights reserved.
doi:10.1016/j.orgel.2011.11.022

tained from *ex-situ* studies. However, indirectly associated with the cell properties of OSCs and are expensive to apply.

This paper reports a real-time technique for monitoring the *in situ* electrical properties of the P3HT:PCBM-based OSCs during thermal annealing. The thermal annealing process was divided into five stages, and the variations of the cell parameters in each stage were explained in detail. The proposed method is practical and useful for optimization, modeling, and in-depth elucidation of the influence of thermal annealing on the performance of OSCs.

2. Experimental

The P3HT (molecular weight ~50,000, regioregularity ~90–94%, 100 mg, purchased from Rieke Metals Inc.) and PCBM (purity >99.5%, 80 mg, purchased from Nano-C, Inc.) were dissolved in chlorobenzene (10 ml, Tedia Company Inc.) with 1:0.8 ratio. The blended solution was stirred for 24 h at 50 °C and deposited (spin-coating at 2000 rpm) on the PEDOT:PSS (~40 nm)-covered and patterned ITO substrate in an N_2-filled glove box. The thickness of the spin-casted layer was ~110 nm. After a 150 nm-thick Al cathode layer was deposited using a thermal evaporator, the samples were transferred back to the glove box and placed on a hot plate. A thin glass was inserted between the metal of hot plate and the OSC device to isolate undesired electrical noise from hot plate. To minimize the degradation of device by UV light, white light-emitting diode (LED) that was composed of blue LED and yellow phosphor with a maximum power of 5 mW was used as the light source, instead of the standard solar simulator. The absorption spectrum of the active layer covers the emission spectrum of the LED. The power of the light and the time interval between measurements were carefully chosen to minimize the decay of the PCE (<3%) of the device under multiple measurements and long-term irradiation. The current–voltage relationship of the OSC device was recorded per 30 s automatically by Agilent 5270B precision source-meter module. The whole process was free of oxygen and H_2O (O_2, H_2O <1 ppm). The irradiated area of the device was ~0.065 cm^2.

3. Results and discussion

In situ monitoring was applied to the as-prepared P3HT:PCBM OSC devices at 165 °C. Fig. 1a shows the temperature profile during thermal annealing. The device was heated from room-temperature (RT) to 165 °C at a constant ramping rate (~14.7 °C/min), held for 30 min, linearly cooled to 127 °C (~3.8 °C/min), and quickly cooled to room temperature (20 °C/min). Based on the variation in the cell parameters (Fig. 1b–e), the thermal annealing process was divided into five stages. (I) The open-circuit voltage (V_{OC}) dropped, but the short-circuit current (J_{SC}), fill factor (FF) and PCE increased as the temperature increased from RT to 127 °C, which is the glass transition temperature of P3HT. (II) All of the parameters increased with temperature from 127 to 165 °C. (III) When the temperature was held at 165 °C for 30 min, J_{SC} increased slightly for the first 7 min, and then remained constant. V_{OC} and FF were unchanged, causing the PCE to increase slightly in the first few minutes. (IV) In this stage, the temperature was decreased from 165 to 127 °C, which is the turning point of V_{OC} during ramping up. All of the parameters except for FF increased gradually. (V) As the temperature was decreased to RT, all of the cell parameters decreased, except for V_{OC}. The variation of FF was similar to that of J_{SC}, except it was constant in stage IV (Fig. 1e). The series resistance (R_S) was associated with the FF through the relationship, $FF_s = FF_0(1 - r_s)$, where FF_0 is the ideal fill factor [12]. Consequently, the PCE increased in stages (I), (II) and (IV), and particularly in the first two stages.

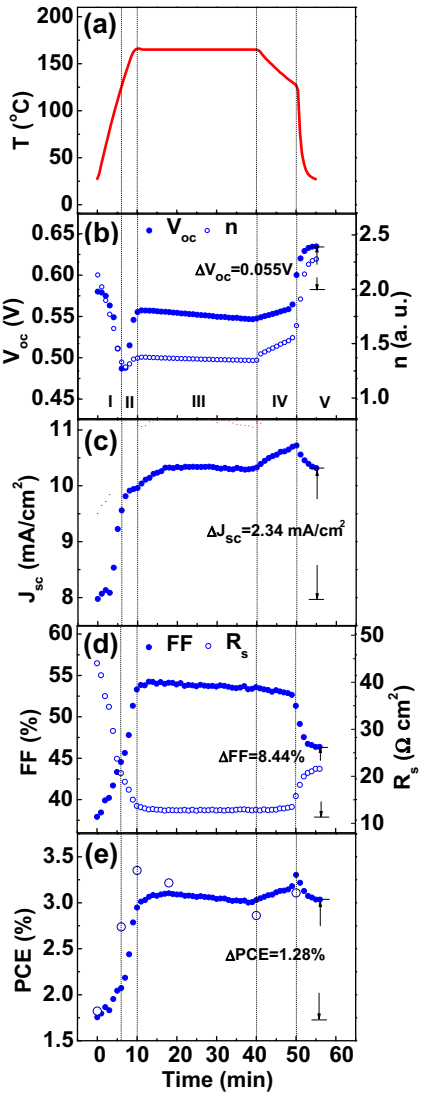

Fig. 1. (a) Temperature profile of thermal annealing. *In situ* curves of (b) V_{OC} and ideality factor n, (c) J_{SC}, (d) FF and R_S, and (e) PCE. △ Indicates net change of cell parameters. Open circles in (e) display PCE values measured *ex situ* after quenching samples from elevated temperature.

To verify the turning of V_{OC} in the ramping up stages, *in situ* measurements were made on several devices that were fabricated using the same process but different annealing temperatures. Fig. 2 shows the curves of V_{OC}

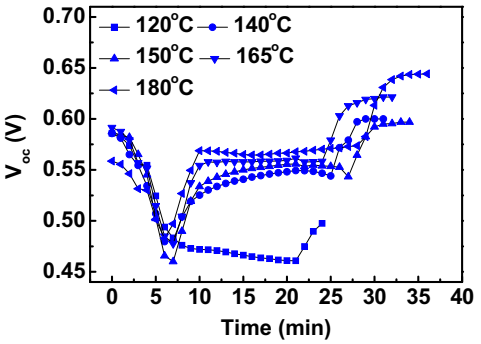

Fig. 2. *In situ* V_{OC} changes in several annealing temperatures.

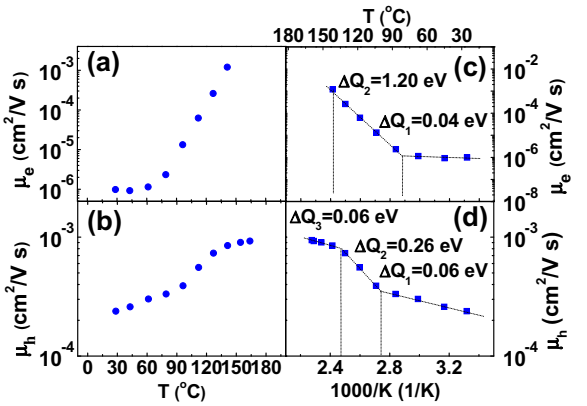

Fig. 3. *In situ* variation of (a) electron and (b) hole mobilities of OSCs during thermal annealing. (c) and (d) are Arrhenius plots corresponding to (a) and (b). Activation energy (ΔQ) of each step was labeled.

measured *in situ*. Interestingly, 127 °C marked the turning point of V_{OC} for all of the samples that were annealed at elevated temperatures (>127 °C). Moreover, only those devices exhibited an increase in V_{OC} upon annealing.

The charge generation, recombination and transport in organic blends have been known to strong temperature-dependent. These fact imposes severe restricts to interpret the measured data. One of the fundamental temperature-dependent properties of a diode is the ideality factor (n) [13,14]. The temperature-dependent V_{OC} can be correlated to n by the following equation [15],

$$V_{oc} = \frac{nk_BT}{q} \ln\left(\frac{I_{sc}}{I_0} + 1\right), \quad (1)$$

where k_B is the Boltzmann constant, and I_{SC} and I_0 are the short-circuit current and reverse saturation current, respectively. In stage I, V_{OC} and n decreased as the temperature increased (Fig. 1b). Because the temperature was low, the variation of n is directly associated with V_{OC} through Eq. (1). In stage II, n was almost constant and V_{OC} increased with temperature, indicating that the phase separation of P3HT started to contribute to the V_{OC}. The increase of V_{OC} in the rapid cooling stage (V) was the reverse of the process stage I, but without any changes in the microstructure of the active layer. Hence, the increase in V_{OC} during thermal annealing was identified to mostly in stages II and IV.

The initial increase in J_{SC} (Fig. 1d) was further investigated by *in situ* monitoring of the dark current–voltage (I–V) relations of the electron-only (ITO/Cs_2CO_3/P3HT:PCBM/Al) and hole-only (ITO/PEDOT:PSS/P3HT:PCBM/MoO_3/Al) devices. This observation gave transport behaviors of carriers. Fig. 3a and b shows the mobilities of electrons (μ_e) and holes (μ_h), which were derived from the I–V relationship and the space-charge limiting current model [16,17]. The rapid increase in μ_e started at ~73 °C, indicating that the release of bottle-necking of the blend arose from the clustering of PCBM. On the other side, the rapid increase in μ_h started at ~93 °C, and was associated with the crystallization of P3HT. Because J_{SC} was proportional to $(n_e\mu_e + n_h\mu_h)$, where n_e and n_h denote the concentrations of electrons and holes, the fast increase in mobilities of electrons and holes in the range ~70–140 °C was responsible for the initially rapid increase in J_{SC} (Fig. 1d). Fig. 3c and d presents the Arrhenius plots that correspond to Fig. 3a and b, respectively. From RT to 160 °C, the value of μ_e rises in two linear stages, while the value of μ_h rises in three, indicating that the transport of electrons and holes in each linear step was thermally-activated. The transport of carriers satisfies μ_h (or $\mu_e \propto e^{-\Delta/k_BT}$), where ΔQ is the activation energy and is labeled in Fig. 3c and d.

The *in situ* monitoring clearly elucidated the influence of thermal annealing process in detail and enabled the device to be optimized efficiently. For example, the PCE became constant 7 min after the beginning of stage III, suggesting that 7 min is the possible optimal time for thermal annealing. The *in situ* data was compared with the *ex-situ* data that was measured after quenching the device from different stages. The data measured *ex situ* was plotted in the Fig. 1e (open circle), fitting well with the *in situ* data except that the time to obtain the optimal PCE advanced a little. The difference was ascribed to the unintentionally variation in process and annealing at initial cooling stage, as the variation that was revealed in stage IV. This result was consistent with Xue's observation [18]. Moreover, stage II importantly improved the PCE, indicating that the ramping rate and time scale was also an important factor in optimizing the thermal annealing of a device. With the aid of the *in situ* measurements, the OSCs are easily optimized by tuning each step of the thermal annealing process. Although the proposed method lack for direct observation of morphology, microstructure, and crystallinity of organic, it provides direct information of cell parameters.

Finally, *in situ* photovoltaic measurements were made on devices that were fabricated using exactly the same process but were solvent-annealed after spin casting. This study demonstrated the effectiveness of the *in situ* monitoring method and provided useful information to the wildly concerned phenomenon. Fig. 4 shows the two quite different *in situ* curves. Before thermal annealing, the PCE, V_{OC}, and J_{SC} of the solvent-annealed device were higher than those of the reference (taken from Fig. 1). This fact is known to be associated with the alignment of the P3HT molecules during solvent annealing [4]. The PCE of

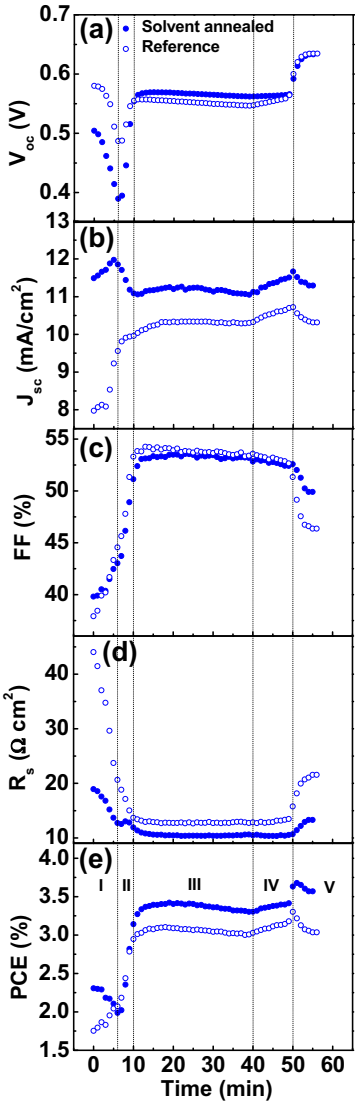

Fig. 4. *In situ* (a) V_{OC} and ideality factor n, (b) J_{SC}, (c) FF, (d) R_S, and (e) PCE during thermal annealing. Division of stages I–V by dotted line is the same as Fig. 1. Solid circles present solvent-annealed device; hollow circles are taken from Fig. 1 as reference (without solvent annealing).

the solvent-annealed device was decreased in stage I and became close to that of the reference because the increase in J_{SC} was smaller than that of the reference. In stage II, the PCE of the solvent-annealed sample exceeded that of the reference because V_{OC} increased faster than the reference, although J_{SC} decreased. The symmetric J_{SC} versus time curve indicated that the variation of the J_{SC} is an effect only of temperature, and is independent of any microscopic or macroscopic changes of the device. In stage IV, FF of the solvent-annealed device dropped less than that of the reference. Therefore, thermal annealing increased the PCE of the solvent-annealed OSC because V_{OC} and FF increased in stages II and IV, regardless of J_{SC}.

4. Conclusion

In conclusion, this study reported on the *in situ* monitoring of the photovoltaic and transport properties of P3HT:PCBM-based OSCs during thermal annealing. The thermal annealing process was divided into five stages, and the improvement of PCE was found to have been associated mostly with the changes that occurred in stages I, II and IV. A dip of the open-circuit voltage (V_{OC}) was observed at the glass transition temperature of P3HT (~127 °C), which temperature is critical to the improvement of V_{OC}. The *in situ* monitoring of the electron/hole transport explained the initial variation of J_{SC} and was thermally activated process. Finally, *in situ* measurements were made to compare the devices with and without solvent annealing.

Acknowledgment

This work was supported by the National Science Council under Contract No. 100-2622-E-006-021-CC3.

References

[1] W. Ma, C. Yang, X. Gong, K. Lee, A. Heeger, Adv. Funct. Mater. 15 (2005) 1617.
[2] M. Reyes, K. Kim, D.L. Carroll, Appl. Phys. Lett. 87 (2005) 083506.
[3] G. Li, V. Shrotriya, J. Huang, Y. Yao, T. Moriarty, K. Emery, Y. Yang, Nat. Mater. 4 (2005) 864.
[4] V. Shrotriya, Y. Yao, G. Li, Y. Yang, Appl. Phys. Lett. 89 (2006) 063505.
[5] Y. Yao, J. Hou, Z. Xu, G. Li, Y. Yang, Adv. Funct. Mater. 18 (2008) 1783.
[6] Y. Zhao, Z. Xie, Y. Qu, Y. Geng, L. Wang, Appl. Phys. Lett. 90 (2007) 043504.
[7] Y. Huang, S. Chuang, M. Wu, H. Chen, C. Chen, W. Su, J. Appl. Phys. 106 (2009) 034506.
[8] S. Miller, G. Fanchini, Y. Lin, C. Li, C. Chen, W. Su, M. Chhowalla, J. Mater. Chem. 18 (2008) 306.
[9] M. Shin, H. Kim, J. Park, S. Nam, K. Heo, M. Ree, C. Ha, Y. Kim, Adv. Funct. Mater. 20 (2010) 748.
[10] T. Agostinelli, S. Lilliu, J. Labram, M. Quiles, M. Hampton, E. Pires, J. Rawle, O. Bikondoa, D. Bradley, T. Anthopoulos, J. Nelson, J. Macdonald, Adv. Funct. Mater. 21 (2011) 1701.
[11] B. Paci, A. Generosi, V. Albertini, P. Perfetti, R. Bettignies, M. Firon, J. Leroy, C. Sentein, Appl. Phys. Lett. 87 (2005) 194110.
[12] M. Green, Solid State Electron 8 (1982) 788.
[13] K.P. O'Donnell, X. Chen, Appl. Phys. Lett. 58 (1991) 2924.
[14] Y.S. Lin, J.J. Jiang, IEEE T. Electron Dev. 56 (2009) 2945.
[15] E. Katz, D. Faiman, S. Tuladhar, J. Appl. Phys. 91 (2001) 5343.
[16] Y. Huang, Y. Liao, S. Li, M. Wu, C. Chen, W. Su, Sol. Ener. Mater. Solar Cells 93 (2009) 888.
[17] C.F. Shih, K.T. Hung, C.Y. Hsiao, K.T. Huang, S.H. Chen, Appl. Phys. Lett. 98 (2011) 113307.
[18] B. Xue, B. Vaughan, C.H. Poh, K.B. Burke, L. Thomsen, A. Stapleton, X. Zhou, G.W. Bryant, W. Belcher, P.C. Dastoor, J. Phys. Chem. C 114 (2010) 15797.